Available online at www.sciencedirect.com
ScienceDirect
Cement and Concrete Research 38 (2008) 794–802
Cement and Concrete Research

Multi-phase hydration model for prediction of hydration-heat release of blended cements

Klaus Meinhard [a,*], Roman Lackner [a,b]

[a] Institute for Mechanics of Materials and Structures, Vienna University of Technology, Karlsplatz 13/202, A-1040 Vienna, Austria
[b] FG Computational Mechanics, Technical University of Munich, Arcisstrasse 21, D-80333 Munich, Germany

Received 28 December 2006; accepted 22 January 2008

Abstract

Recently, the heat release during cement hydration and the so-caused temperature rise was exploited for (i) identification of material properties of early-age cement-based materials (stiffness, strength), and (ii) determination of the diameter and the cement content of jet-grouted structures. In this paper, the underlying hydration model for determination of the heat release and its rate is refined for Ordinary Portland Cements (OPC) and extended towards blended cements. Hereby, the overall degree of hydration with one kinetic law is replaced by a multi-phase hydration model, taking the hydration kinetics of the main clinker phases into account. As regards blended cements, which are commonly used in engineering practice, the effect of slag hydration is incorporated into the presented multi-phase model. The developed hydration model for both plain and blended cement is validated by means of differential-calorimetry (DC) experiments.

Keywords: Calorimetry; Hydration; Kinetics; Blended cement; Granulated; Blast-furnace slag

1. Introduction

The chemical reactions taking place during the hydration process are described by the stoichiometric reactions of the four main clinker phases of Portland cement[1] [Tricalciumsilicate (C_3S), Dicalciumsilicate (C_2S), Tricalciumaluminate (C_3A), and Tetracalciumaluminateferrite (C_4AF)] [1]:

$$C_3S + 5.3H \rightarrow 0.5C_{3.4}S_2H_8 + 1.3CH \quad (1)$$

$$C_2S + 4.3H \rightarrow 0.5C_{3.4}S_2H_8 + 0.3CH \quad (2)$$

$$C_3A + 3C\bar{S}H_2 + 26H \rightarrow C_6A\bar{S}_3H_{32} \quad (3)$$

$$C_3A + 0.5C_6A\bar{S}_3H_{32} + 2H \rightarrow 1.5C_4A\bar{S}H_{12} \quad (4)$$

$$C_3A + CH + 12H \rightarrow C_4AH_{13} \quad (5)$$

$$C_4AF + 2CH + 10H \rightarrow 2C_3(A,F)H_6 \quad (6)$$

Eqs. (3)–(5) describe the formation of calcium aluminate hydrates (C–A–H) from C_3A in the presence of gypsum. In general, the latter is added in order to delay setting of C_3A. Initially, C_3A reacts with gypsum to form ettringite, see Eq. (3). After all gypsum is consumed, C_3A reacts with the previously formed ettringite to form monosulfoaluminates, see Eq. (4). Following depletion of the ettringite supply, C_3A reacts with portlandite (CH), which is one of the products of C_3S and C_2S hydration, see Eqs. (1) and (2).

Already in the mid-1990s an overall degree of hydration ξ was introduced in order to compute the hydration extent, representing the entire set of chemical reactions, with $\xi=0$ at the start of hydration and 1 at complete hydration. More recently, four degrees of hydration, referring to the main clinker phases (ξ_{C_3S}, ξ_{C_2S}, ξ_{C_3A}, and ξ_{C_4AF}, with $0 \le \xi_x \le 1$), were introduced [2]. The hydration kinetics of each clinker phase x is given by nucleation and growth laws that link the reaction rate

* Corresponding author. Tel.: +43 1 58801 20241; fax: +43 1 58801 20298.
E-mail address: klaus.meinhard@tuwien.ac.at (K. Meinhard).

[1] Throughout this paper standard cement chemistry abbreviations were used, with C=CaO, S=SiO_2, A=Al_2O_3, F=Fe_2O_3, $\bar{S}$=SO_3, H=H_2O, M=MgO, Na=NaO and F=Fe_2O_3.

0008-8846/$ - see front matter © 2008 Elsevier Ltd. All rights reserved.
doi:10.1016/j.cemconres.2008.01.008

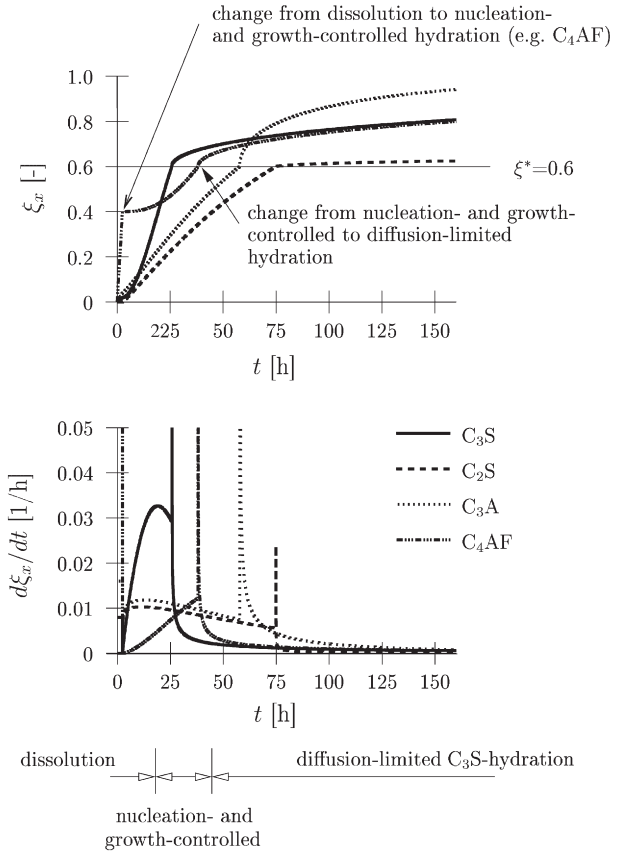

Fig. 1. ξ_x and $d\xi_x/dt$ for the four main clinker phases for $\xi^*=0.6$ (water/cement-ratio=0.3; temperature=293 K; average particle size r_p=7 μm).

$d\xi_x/dt$ to the respective driving force of the chemical reaction (chemical affinity $\tilde{A}(\xi_x)$), reading in dimensionless form

$$\tau_x \frac{d\xi_x}{dt} = \tilde{A}(\xi_x), \tag{7}$$

where τ_x is the characteristic time associated with the reaction. For the three stages of the hydration process [(a) induction, (b) nucleation/growth, and (c) diffusion], the following kinetic laws were proposed in [2]:

(a) Induction (dissolution of the clinker phases until $t=t_{x,0}$ and $\xi=\xi_{x,0}$): Given the relatively short period, the process is simulated by a constant reaction rate, i.e. $\tilde{A}=1$ and $\tau_x=\tau_{x,0}=t_{x,0}/\xi_{x,0}$, where $t_{x,0}$ is the duration of the induction period and $\xi_{x,0}$ is the hydration threshold of clinker phase x at the end of the induction period.

(b) Nucleation/growth (nucleation- and growth-controlled hydration of clinker phases until the critical hydration degree $\xi=\xi_x^*$): this process is simulated by the Avrami model, commonly employed in cement chemistry, with

$$\xi_x = 1 + \xi_{x,0} - \exp[-a^\kappa] \tag{8}$$

and

$$\frac{d\xi_x}{dt} = \exp[-a^\kappa]\kappa a^{\kappa-1}\frac{1}{\kappa\tau_0 \mathrm{Arr}}, \tag{9}$$

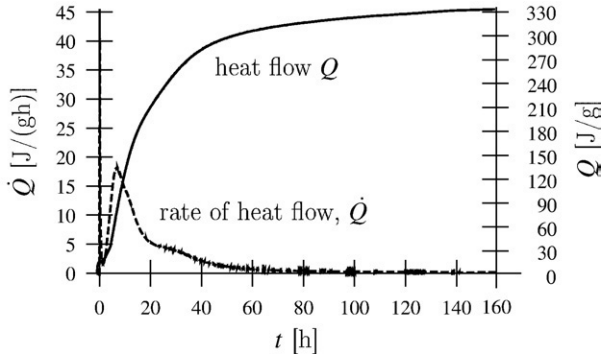

Fig. 2. Output of DC test: history of heat-flow rate $\dot{Q}$ and heat flow Q.

where $a=(t-t_0)/(\kappa\tau_0\mathrm{Arr})$ and $\mathrm{Arr}=\exp[E_{ax}/R(1/T-1/T_0)]$, where E_{ax} is the activation energy parameter for the x-th clinker phase and R is the universal gas constant (8.314 J/(mol K)). In Eqs. (8) and (9), κ is the Avrami parameter [2] and τ_0 is the characteristic time of the nucleation/growth process at reference temperature T_0, with T_0=293 K. According to [2], $E_{a,C_3S}/R$, $E_{a,C_2S}/R$, $E_{a,C_3A}/R$, $E_{a,C_4AF}/R$ were set equal to 4500, 2500, 5500, and 4200.

(c) Diffusion (diffusion-controlled hydration beyond $\xi=\xi_x^*$): beyond ξ_x^*, the kinetics of the hydration reactions is limited by diffusion of dissolved ions through the layers of hydrates formed around the clinker. According to [3],

$$\xi_x = 1 - \left(-\frac{\sqrt{2D(t-t_x^*)}}{r_p\sqrt{\mathrm{Arr}}\sqrt{\Phi_0/\Phi}} + \sqrt[3]{1-\xi_x^*}\right)^3 \tag{10}$$

and

$$\frac{d\xi_x}{dt} = -3\left(-\frac{\sqrt{2D(t-t_x^*)}}{r_p\sqrt{\mathrm{Arr}}\sqrt{\Phi_0/\Phi}} + \sqrt[3]{1-\xi_x^*}\right)^2\left(\frac{-\sqrt{2D}(t-t_x^*)^{-1/2}}{2r_p\sqrt{\mathrm{Arr}}\sqrt{\Phi_0/\Phi}}\right), \tag{11}$$

where D is a diffusion coefficient (values given in [2] for each clinker phase, depending on w/c-ratio), r_p is the average particle size, Φ_0 is the specific surface area of the cement used for determination of the parameters of the kinetic model of the four clinker phases [2], with Φ_0=3602 cm^2/g, and Φ is the specific surface area of the investigated type of cement.

Table 1
Composition (in [mass%]) and properties of investigated types of cement (r_p [μm]: average particle size, Q_∞ [J/g]: total heat release at the end of hydration, W_n [1]: maximum amount of bound water present in fully-hydrated cement)

Component	m_x [mass%]
C_3S	62.2
C_2S	10.9
C_3A	8.1
C_4AF	6.7
Gypsum	7.4
Q_∞[J/g]	475
W_n [−] according to Eq. (14)	0.22

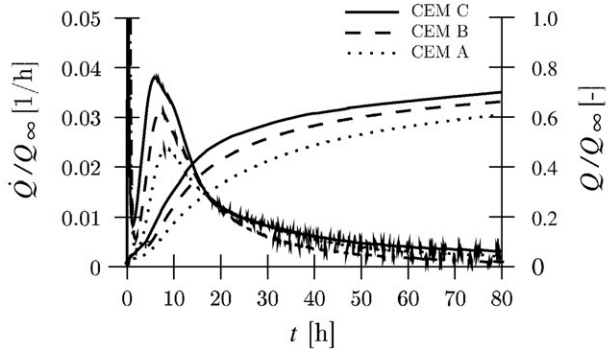

Fig. 3. DC-test results: heat flow Q and heat-flow rate $\dot{Q}$ for CEM A to CEM C (Q_∞ according to Table 1).

Fig. 1 shows the evolution of the degree of hydration of the four main clinker phases C_3S, C_2S, C_3A, and C_4AF obtained from application of the multi-phase hydration model outlined in [2] to each of the four main clinker phases and the evolution laws (7)–(11), considering water/cement-ratio of 0.3 and an average particle size of r_p=7 μm. The earlier described stages in the evolution of the degree of hydration, i.e., dissolution, nucleation/growth, and diffusion can be identified by the shape of the curves given in Fig. 1. The constant hydration rate of the dissolution process results in a linear increase from ξ=0 to $\xi_x=\xi_{x,0}$. Beyond this value, hydration is controlled by nucleation/growth until $\xi_x=\xi_x^*$ [2]. The diffusion-limited hydration shows a decreasing rate, with $d\xi_x/dt=\infty$ at the beginning of the diffusion-controlled hydration (see Fig. 1).

In the following section, the performance of the outlined multi-phase hydration model is assumed for OPC by calorimetry tests conducted at 30 °C and 50 °C. The extension and validation of the multi-phase hydration model to blended cements is presented in Section 3. Section 4 contains concluding remarks.

2. Differential-calorimetry (DC) tests

In order to investigate the performance of the multi-phase hydration model described in previous section, the heat release of hydrating cement was monitored by means of DC. Hereby, water and cement are mixed in the test chamber and the heat flux and the heat-flux rate required to keep the hydrating sample at a pre-specified (constant) temperature are recorded from the first moment of reaction. DC tests were performed at temperatures of 30 °C and 50 °C, with samples consisting of 6.0 g cement and 3.0 to 3.6 g water (water/cement-ratio ranging from 0.5 to 0.6). The energy required to keep the pre-specified temperature is monitored for both an inert reference sample and the hydrating sample, giving the heat flow $Q(t)$ [J/g] associated with the hydration process, see Fig. 2.

Table 2
Released heat for clinker phases according to [4]

	Q_x [J/g]		Q_x [J/g]
C_3S	500	C_4AF	420
C_2S	250	C_3A	1340

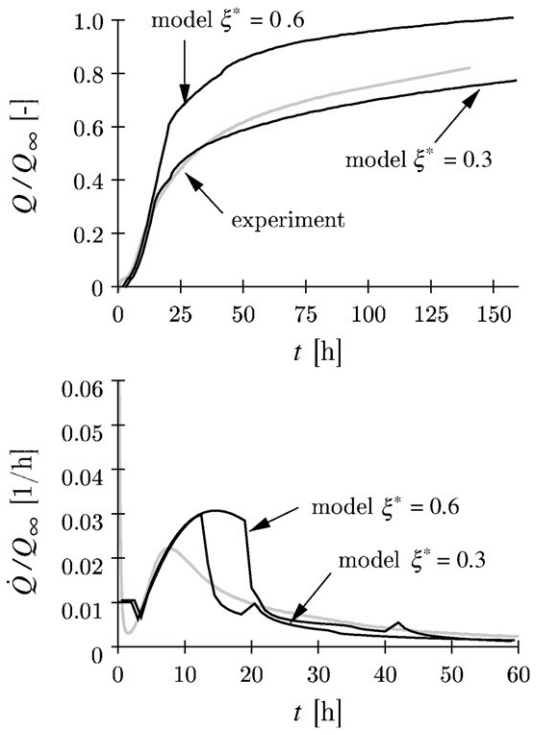

Fig. 4. Heat flow Q and heat-flow rate $\dot{Q}$ for CEM A (Q_∞=475 J/g): experimental data compared with result from multi-phase hydration model with ξ^*=0.3 and 0.6 (water/cement-ratio set equal to 0.22).

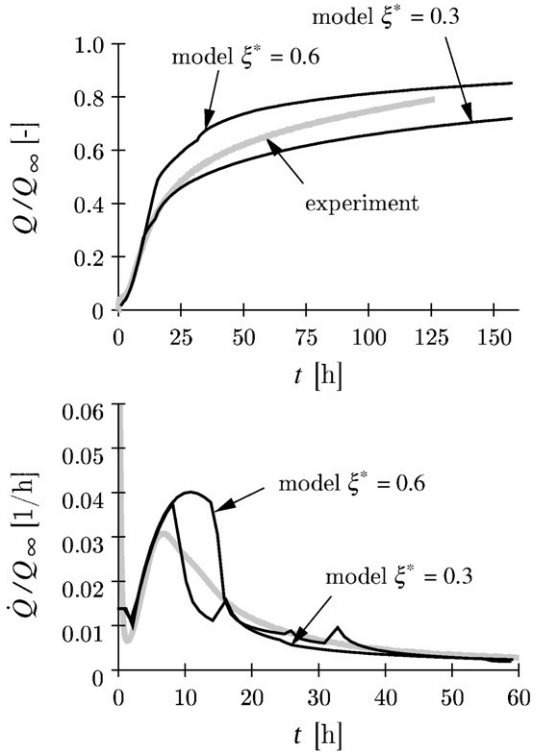

Fig. 5. Heat flow Q and heat-flow rate $\dot{Q}$ for CEM B (Q_∞=475 J/g): experimental data compared with result from multi-phase hydration model with ξ^*=0.3 and 0.6 (water/cement-ratio set equal to 0.22).

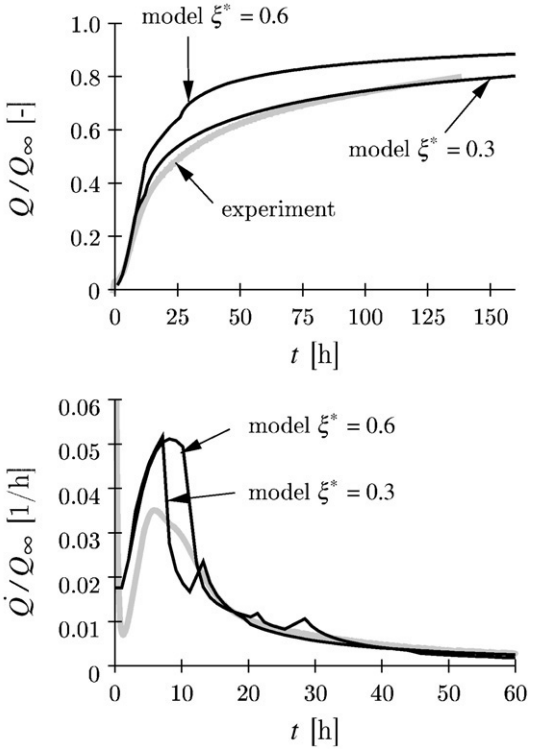

Fig. 6. Heat flow Q and heat-flow rate $\dot{Q}$ for CEM C (Q_∞=475 J/g): experimental data compared with result from multi-phase hydration model with ξ^*=0.3 and 0.6 (water/cement-ratio set equal to 0.22).

The multi-phase hydration model was applied to three laboratory cements. These cements (referred to as CEM A to CEM C) were produced in the same cement company, showing the same chemical and mineralogical composition. Values for specific surface area of the cement equal 3190, 4000, and 4800 [cm^2/g], and mean particle radius r_p equal to 10, 7, and 5 μm are given for CEM A, B, and C, respectively. The mass fractions m_x of each clinker phase and gypsum are given in Table 1. Other oxides in the raw material, e.g., free CaO, MgO, Na_2O_3, are not considered within the employed multi-phase hydration model.

Fig. 3 shows the experimentally obtained heat flow $Q(t)$ and the heat-flow rate $\dot{Q}$(t), both related to the heat flow Q at $t=\infty$, Q_∞. The latter is computed from the heat release associated with the hydration of the different clinker phases, with $Q_\infty=(\Sigma_x m_x Q_x)/(\Sigma_x m_x)$, using the parameters given in Tables 1 and 2. The so-obtained values for Q_∞ are given in Table 1.

Table 3
Composition of GGBFS according to [7]

Oxide	mass%	Oxide	mass%
S	33.9–38.1	K	0.31–0.72
C	36.6–42.8	Na	0.20–0.45
A	8.8–13.3	$\overline{S}$	0.0–2.4
M	6.7–12.8		
Glass content	89–99		
Sulfid content	0.8–1.3		
(C+M)/S-ratio	1.27–1.47		
(C+M+A)/S-ratio	1.53–1.85		

Table 4
Oxides in slag glass [mass%] for the two slags produced in Austria

	Oxides included in slag glass					
	y_C	y_S	y_A	y_M	y_S	y_F
Donawitz	37.7	34.1	11.6	9.9	0.7	1.0
Linz	35.9	37.9	11.6	8.9	2.5	0.45

The experimentally-obtained results are compared with the output of the multi-phase hydration model. As regards the latter, the heat flow and the heat-flow rate are obtained from

$$Q(t) = \frac{\Sigma_x m_x \xi_x(t) Q_x}{\Sigma_x m_x} \tag{12}$$

and

$$\frac{dQ}{dt} = \frac{\Sigma_x m_x d\xi_x/dt Q_x}{\Sigma_x m_x}, \tag{13}$$

where Q_x [J/g] represents the released heat of the clinker phase x (see Table 2). The obtained results are shown in Figs. 4–6. In addition to ξ^*=0.6 [2], simulation results with ξ^*=0.3 are included, giving a better agreement between simulation results and the DC-test data.[2] Whereas the amount of cement and water used in the DC tests gives a water/cement-ratio of 0.5 to 0.6, the water/cement-ratio used in the hydration model was related to the maximum amount of bound water present in fully-hydrated cement, with

$$W_n(t) = \sum_x W_x m_x \xi_x(t), \tag{14}$$

where W_x [(g water)/(g clinker phase x)] is the amount of bound water related to the amount of clinker phase x, giving water/cement-ratios in the range of 0.2 to 0.3. According to [6], W_{C_3S}, W_{C_2S}, W_{C_3A}, and W_{C_4AF} were set equal to 0.234, 0.178, 0.514, and 0.158.

3. Multi-phase hydration model for blended cement

In order to reduce costs in engineering practice, blended cements consisting of OPC and, e.g., blast-furnace slag, silicate fume, lime-stone are used. In this section, the multiphase hydration model used in the previous section is extended towards OPC mixed with ground granulated blast-furnace slag (GGBFS). GGBFS is formed between 1350–1550 °C in the manufacturing process of steel, when limestone reacts with material rich in S_iO_2 (S) and Al_2O_3 (A) associated with the ore or present in the ash of the coke. If cooled rapidly below 800 °C, which is performed by spraying droplets of the molten slag with high-pressure jets of water, a wet, sandy material is obtained which, when dried and ground, gives GGBFS, containing over

[2] In fact, the decreased value of ξ^* was taken from [5], where the range of ξ^*(the shift from nucleation-growth to diffusion-limited hydration) was specified from 0.3 to 0.4.

Table 5
Products of slag hydration [g/(1000 g slag glass)], S/C-ratio and A/C-ratio for the two slags produced in Austria (values in brackets are mass-%)

	Hydration products						
	N_{C-S-H}	$N_{M_{4.5}AH_{13}}$	$N_{C_6AFS_2H_8}$	$N_{C_6A\bar{S}_3H_{32}}$	S/C	A/C	W_n
Donawitz	840 (69.0)	284 (23.4)	54 (4.5)	36 (3.0)	0.899	0.081	0.21
Linz	843 (67.0)	253 (20.2)	24 (1.9)	133 (10.6)	1.117	0.092	0.25

95% of glass. Similar to cementitious materials, slag glass can be considered as a system of C–A–S, see Table 3.

3.1. Hydration of GGBFS

GGBFS reacts in highly alkaline solution and/or in liquids containing CH as e.g. provided by the hydration of C_3S and C_2S in blended cements [8]. According to [9], a coating of aluminosilicate forms on the surface of slag grains within a few minutes of exposure to water. This coating is impermeable to water and unless a chemical activator is present, further hydration is inhibited. Portland cement, gypsum, and many alkalies have been used as such activator and, generally, the rate of hydration is faster at high alkaline concentrations.

For a pH lower than 11.5, the equilibrium solubility of silica is low and GGBFS simply does not dissolve. When mixed with an aqueous phase with pH higher than 11.5, as present in hydrating cement, the reaction is activated or accelerated. The main hydration products of GGBFS hydration are C–S–A–H, hydrotalcite (M_5AH_{13}), and ettringite ($C_6A\bar{S}_3H_{32}$). In addition to the main products, tetracalcium aluminate hydrate (C_4AH_{13}), straetlingite (C_2ASH_8), and hydrogarnet ($C_6AFS_2H_8$) are formed [10,11], reading

$$C–S–A–M–\bar{S}–F + H \rightarrow C–S–A–H + M_5AH_{13} + C_6AFS_2H_8 + C_6A\bar{S}_3H_{32} + C_2ASH_8 + C_4AH_{13}. \quad (15)$$

According to [11],

- the amount of hydrotalcite, hydrogarnet, and ettringite follows from the oxide content of M, F, and $\bar{S}$ in the slag, respectively;
- A, which is present in the slag, is first combined with M, F, and $\bar{S}$ to form the hydrotalcite, hydrogarnet, and ettringite, whereas the remaining A substitutes S installed during C–S–H formation;
- the limit of A substitution in C–S–H is related to the C/S-ratio of the raw slag glass. When there is sufficient A from the slag to achieve the maximum substitution, the remaining A reacts to tetracalcium aluminat hydrate (C_4AH_{13}) and/or straetlingite (C_2ASH_8).

Based on the relation between the amount of hydration products formed by slag hydration and the chemical composition of the raw slag material given in [11], the composition of the hydration products for the two Austrian slags (Donawitz and Voest–Linz) can be determined (see Table 4).

C–S–H formed during slag hydration has a lower C/S-ratio (approximately 1.1) than that from the OPC (approximately 1.7). In [11], the amount of hydration products formed by slag hydration is given as a function of the chemical composition of the slag glass (see Table 4). Based on the molar balance of each oxide, the following equations were derived in [11]:

$$y_C = N_{C-S-H} + 6N_{C_6AFS_2H_8} + 6N_{C_6A\bar{S}_3H_{32}} + 4N_{C_4AH_{13}} + 2N_{C_2ASH_8}, \quad (16)$$

$$y_S = aN_{C-S-H} + 2N_{C_6AFS_2H_8} + N_{C_2ASH_8}, \quad (17)$$

$$y_A = bN_{C-S-H} + N_{M_{4.5}AH_{13}} + N_{C_6AFS_2H_8} + N_{C_6A\bar{S}_3H_{32}} + N_{C_4AH_{13}} + N_{C_2ASH_8}, \quad (18)$$

$$y_{\bar{S}} = 3N_{C_6A\bar{S}_3H_{32}}, \quad (19)$$

$$y_M = 4.5N_{M_{4.5}AH_{13}}, \quad (20)$$

$$y_F = N_{C_6AFS_2H_8}, \quad (21)$$

where a and b refer to S/C-ratio and A/C-ratio, respectively. Thus, with the molar composition of oxides in the slag glass at

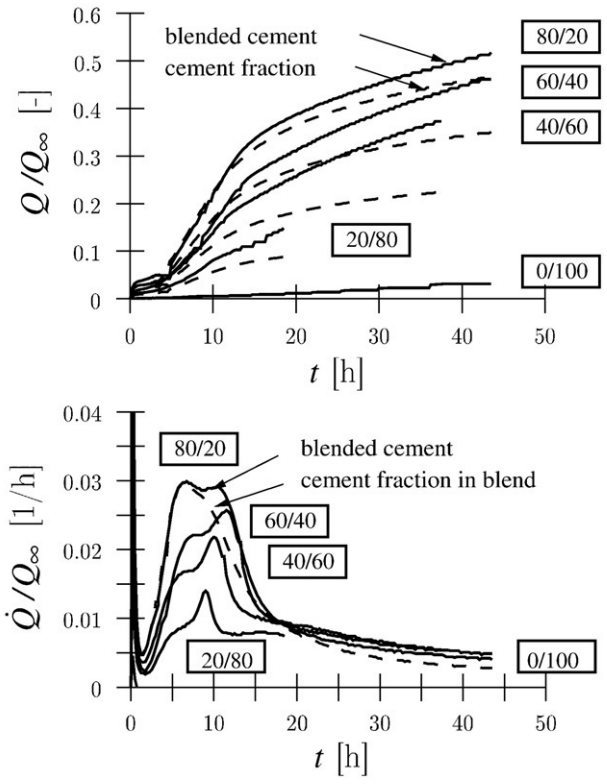

Fig. 7. DC-test results: heat flow Q and heat-flow rate $\dot{Q}$ for different cement/slag-ratios (CEM C/GGBFS, $Q_{\infty,blend}$=468 J/g for all cement blends) at 30 °C.

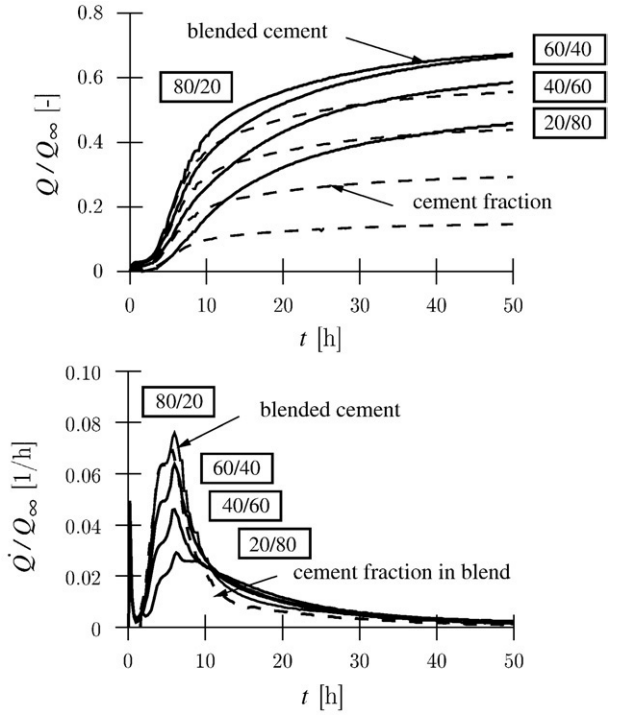

Fig. 8. DC-test results: heat flow Q and heat-flow rate $\dot{Q}$ for different cement/slag-ratios (CEM C/GGBFS, $Q_{\infty,\mathrm{blend}}$=468 J/g for all cement blends) at 50 °C.

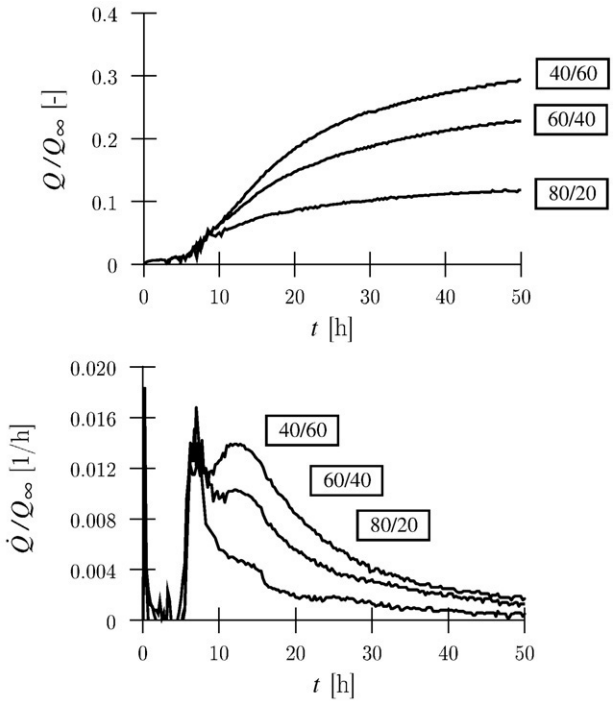

Fig. 10. DC-test results: heat flow Q and heat-flow rate $\dot{Q}$ associated with slag hydration for different cement/slag-ratios (CEM C/GGBFS, $Q_{\infty,\mathrm{blend}}$=468 J/g for all cement blends) at 50 °C.

hand (y_C, y_S, y_A, y_M, $y_{\bar{S}}$, and y_F), the molar composition of the hydration products can be computed, giving N_{C-S-H} (C–S–H phase), $N_{M_{4.5}AH_{13}}$ (hydrotalcite), $N_{C_6AFS_2H_8}$ (hydrogarnet), $N_{C_6A\bar{S}_3H_{32}}$ (ettringite), $N_{C_4AH_{13}}$ (tetracalcium aluminate hydrate), and $N_{C_2ASH_8}$ (straetlingite). The so-obtained molar composition of the hydration products, C/S-ratio and A/C-ratio for the two slags available in Austria are given in Table 5 which were determined following the evaluation scheme presented in [11], where $N_{C_4AH_{13}}$ and $N_{C_2ASH_8}$ were set equal to zero.

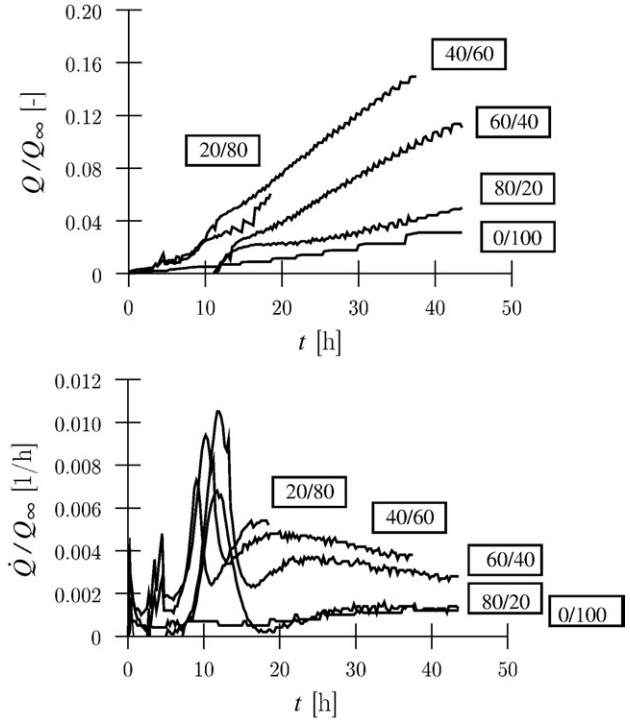

Fig. 9. DC-test results: heat flow Q and heat-flow rate $\dot{Q}$ associated with slag hydration for different cement/slag-ratios (CEM C/GGBFS, $Q_{\infty,\mathrm{blend}}$=468 J/g for all cement blends) at 30 °C.

3.2. DC tests

DC tests were performed for blended cements, composed of CEM C (Q_∞=475 J/g) and slag from Donawitz ($Q_{\infty,\mathrm{slag}}$=461 J/g according to [12]), with a cement/slag-ratio ranging from 20/80 to 80/20, see Figs. 7 and 8 for DC tests conducted at 30 °C and 50 °C, respectively.[3] The dashed lines represent the heat flow and heat-flow rate of the respective cement fraction in the cement blend. It was obtained from multiplying the DC-test result for pure cement with the respective amount of cement in the cement blend. Thus, the difference between the solid and dashed line can be considered as the heat release associated with slag hydration, as shown in Figs. 9 and 10.

3.3. Hydration model

According to Figs. 9 and 10, no heat release associated with the hydration of the GGBFS fraction is observed in the first hours after the initiation of the hydration process (t=0 refers to the time instant of mixing the cement blend with water). Two

[3] For the determination of the heat flow and heat-flow rate of blended cements Eqs. (12) and (13) were used, considering in addition to the four clinker phases the mass fraction of the slag, with $Q_{\infty,\mathrm{slag}}$=461 J/g for the considered type of slag, giving $Q_{\infty,\mathrm{blend}}$=468 J/g.

Table 6
Avrami-model parameters and parameters describing the exponential decay for slag hydration of Donawitz GGBFS (T_0=20 °C)

	Aluminum products	C–S–A–H (Avrami)	C–S–A–H (exponential decay)
$\xi_{x,0}$	0	0	0.15
Starting at …	ξ_{cement}=0.14	ξ_{Al}=0.85	ξ_{CSAH}=0.40
Ending at …	ξ_{Al}=0.85	ξ_{CSAH}=0.40	–
$\tau_x(T_0)$ [h]	3	35	90
κ [−]	3.0	1.5	–
E_{ax}/R[K]	3000	5500	5500
Q_∞ [a] [J/g]	20	130	468

[a] Obtained from DC-test results.

peaks are observed in the history of the heat-flow rate, with the first peak within 8 and 14 hours (T=30 °C) and 5 and 10 h (T=50 °C). Surprisingly, the heat-flow rate associated with this peak is approximately the same [3 to 5 J/(gh) (T=30 °C) and 5.5 to 7.5 J/(gh) (T=50 °C)] for all considered cement blends and is, thus, independent of the cement/slag-ratio. The second peak, on the other hand, increases with increasing cement/slag-ratio for all conducted experiments. The heat-release rate associated with the second peak decreases slowly after the peak. The value of the heat-release rate obtained at the end of the conducted DC tests is in good agreement with test results reported in [13], giving a heat-flow rate of $\dot{Q}$=0.72 J/(gh) [$\dot{Q}/Q_\infty$=0.00156 1/h] at $t\approx$80 h for DC tests conducted at T=25 °C.

Based on the obtained DC-test results, the hydration of GGBFS is split, after a period with no heat release, into two chemical reactions associated with the formation of hydration products [11], i.e.,

1. the aluminum reaction, giving the first peak of slag hydration, which is independent of the amount of slag in the blended cement, and
2. the C–S–A–H formation, giving the second peak of slag hydration, which is characterized by rapid increase and a slow decrease of the heat-flow rate, depending on the amount of slag. In contrast to the diffusion-limited decrease of the heat-release rate obtained for the hydration of OPC, the decrease of the heat-release rate associated with C–S–A–H is described by an exponential decay, well-suited to describe the decrease of the amount of slag glass available for slag hydration [14].

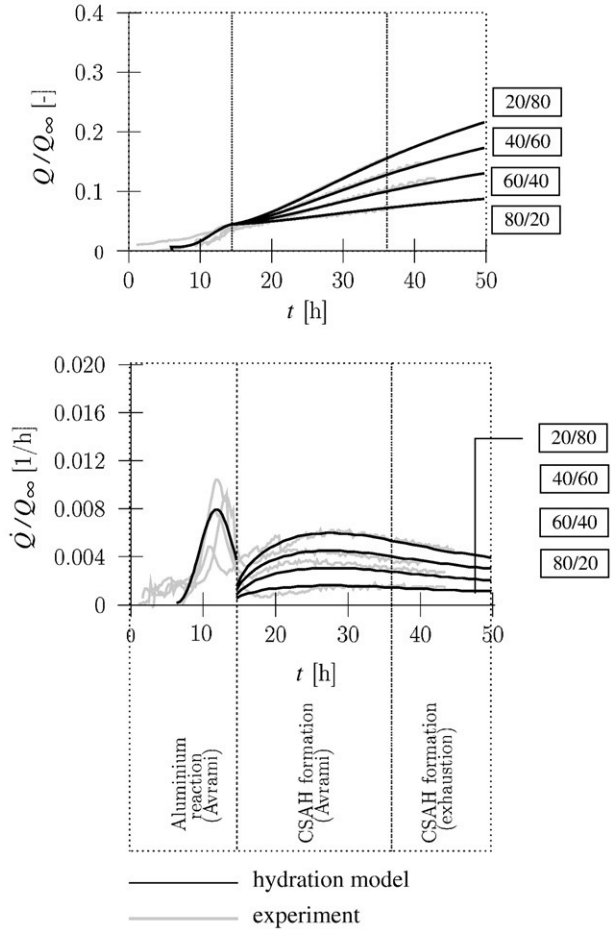

Fig. 11. Heat flow Q and heat-flow rate $\dot{Q}$ for slag fraction in blended cements (CEM C/GGBFS, cement/slag-ratio=80/20, 60/40, 40/60, and 20/80): experimental data compared with result from multi-phase hydration model with ξ^*=0.3, water/cement-ratio=0.22, and T=30 °C.

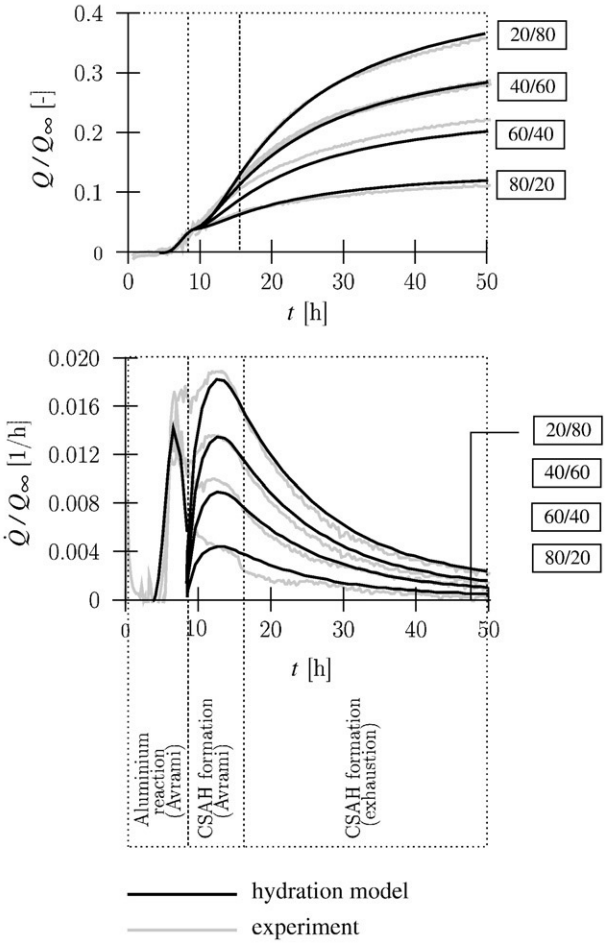

Fig. 12. Heat flow Q and heat-flow rate $\dot{Q}$ for slag fraction in blended cements (CEM C/GGBFS, cement/slag-ratio=80/20, 60/40, 40/60, and 20/80): experimental data compared with result from multi-phase hydration model with ξ^*=0.3, water/cement-ratio=0.22, and T=50 °C.

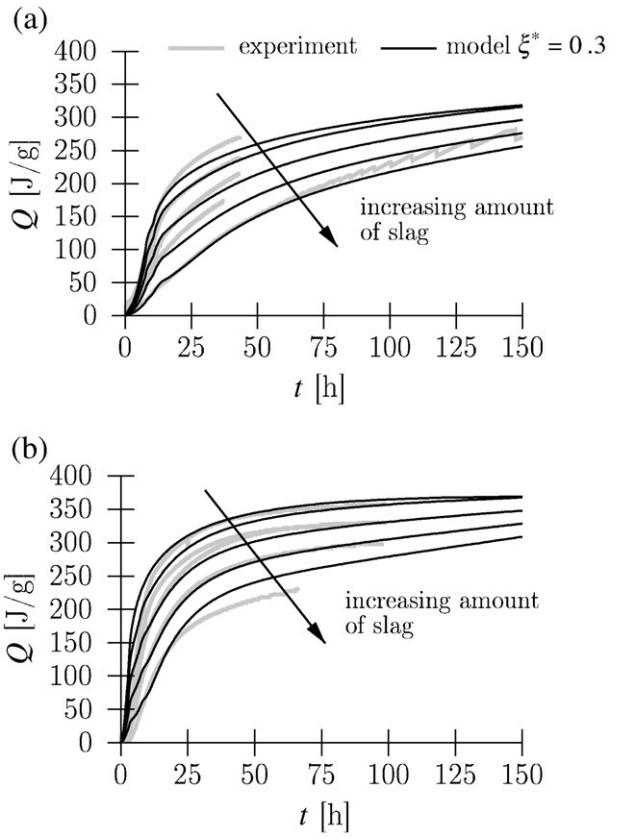

Fig. 13. Heat flow Q for cement blends (CEM C/GGBFS, cement/slag-ratio ranging from 80/20 to 20/80): experimental data compared with result from multi-phase hydration model with $\xi^*=0.3$, water/cement-ratio=0.22 for (a) $T=30$ °C and (b) $T=50$ °C.

In order to account for the heat release associated with slag hydration, the multi-phase hydration model outlined in Section 1 is extended, considering:

- an induction phase, representing the dissolution of the slag glass;
- nucleation- and growth-controlled hydration of the aluminum present in the slag glass;
- nucleation- and growth-controlled hydration followed by an exponential decay of the C–S–A–H formation.

For the description of the nucleation- and growth-controlled hydration related to aluminum reaction and C–S–A–H formation, the Avrami model is employed. Based on the DC-test results, the respective parameters were identified as given in Table 6.[4] Comparison of the heat flow predicted by the extended multi-phase model with DC-test data gives good agreement between experimental data and model prediction for different cement/slag-ratios considered in the experimental program (see Figs. 11–13).

[4] The w/c-ratio in the extended hydration model was related to the maximum amount of bound water present in fully-hydrated cement (see Eq. (14) and Table 1) and in the slag fraction $W_{n,\mathrm{slag}}$, which is equal to 0.21 and 0.25 for slag Donawitz and Linz, respectively. In this paper, W_n is set equal to 0.22 (value for OPC, see Table 1) for all blended cements.

The hydration heat release associated with the exponential decay of the C–S–A–H formation (for $\xi_{\mathrm{CSAH}}\geq 0.4$), is described by

$$\frac{d\xi_{\mathrm{CSAH}}}{dt}=\frac{d\xi_{\mathrm{CSAH},\infty}}{dt}+\left(\frac{d\xi_{\mathrm{CSAH},0.4}}{dt}-\frac{d\xi_{\mathrm{CSAH},\infty}}{dt}\right)\exp\left[-\frac{t-t_{0.4}}{\tau_{\mathrm{CSAH}}}\right], \tag{22}$$

where $t_{0.4}$ is the time instant when $\xi_{\mathrm{CSAH}}=0.4$, $d\xi_{\mathrm{CSAH},0.4}/dt$ is the hydration rate at $t_{0.4}$, τ_{CSAH} [h] is the characteristic time of the exponential decay, and $d\xi_{\mathrm{CSAH},\infty}/dt$ is the asymptote of C–S–A–H formation for GGBFS. As regards the latter, $d\xi_{\mathrm{CSAH},\infty}/dt$ is set equal to $0.005/Q_{\mathrm{slag},\infty}$ [1/h], following the test results given in [7], reporting a degree of slag hydration of 0.30–0.55 for 28 days and 0.45–0.75 for 2 years.

The characteristic time τ_{CSAH} is determined from the history of the degree of hydration provided by the Avrami model at $\xi_{\mathrm{CSAH}}=0.4$ (see Table 6). The value of τ_{CSAH} is temperature dependent, described by an Arrhenius-type law experiment with $E_{a,\mathrm{CSAH}}/R=5500$ K, where $E_{a,CSAH}/R$ was obtained from DC-tests.

4. Concluding remarks

In this paper, the multi-phase hydration model proposed in [2] was extended towards blended cements commonly used in civil engineering applications, dealing with massive structures. Both the original and the extended multi-phase model were assessed and validated by means of differential-calorimetry (DC) tests. From the comparison between model prediction and DC-test results, the following conclusions can be drawn:

- As proposed in [2], the hydration process is diffusion limited for $\xi_x\geq\xi_x^*$. However, the value of ξ_x^* was reduced from 0.6 to 0.3 in order to achieve better agreement between model prediction and test results. The reduced value of ξ_x^* for the change from nucleation-growth to diffusion-limited hydration lies in the range from 0.3 to 0.4 given in [5].
- The hydration of ground granulated blast-furnace slag (GGBFS) may be split into three stages, (a) the induction period, (b) the aluminum reaction, and (c) the C–S–A–H formation. While both the aluminum reaction and the C–S–A–H formation were described by the Avrami model, an additional exponential decay was introduced for the latter. The aluminum reaction was related to the first peak in heat-release history, starting approximately 5 (10) hours after the onset of hydration for a testing temperature of 50 °C (30 °C). At this time, the hydration degree describing the hydration extent of the four main clinker phases contained in the cement fraction included in the cement blend equals 0.14. In contrast to the relatively fast aluminium reaction, the C–S–A–H formation is more slowly, characterized by a long-term heat release, well-described by the aforementioned exponential-decay model.
- Whereas cement hydration is diffusion limited, controlled by diffusion of dissolved ions through the layers of hydration products formed around the clinker, slag hydration is limited by an exponential decay of the concentration of the slag glass

(reactant) with time, representing the decrease of the amount of unhydrated slag glass available for the chemical reactions taking place during hydration.

- The discontinuities observed in the course of the hydration heat release rate determined by using the multi-phase hydration model are caused by the underlying mathematical formulation of the different stages of hydration for each clinker phase. These sharp peaks are artificial and do not occur in reality.

Acknowledgments

The authors thank Reinhard Bünker, Richard Gutsche, Martin Hopfgartner, and Johann Perner (PORR Technobau und Umwelt AG, Abteilung Grundbau, Vienna, Austria) for helpful support and Lafarge CTEC (Mannersdorf, Austria) for supplying the laboratory cement and the blast-furnace slag used in the experimental program. Financial support by the Austrian Research Promotion Agency Ltd. (FFG) under project 809215 is gratefully acknowledged.

References

[1] P.D. Tennis, M. Jennings, A model for two types of calcium silicate hydrate in the microstructure of Portland cement pastes, Cement and Concrete Research 30 (2000) 855–863.
[2] O. Bernard, F.-J. Ulm, E. Lemarchand, A multiscale micromechanics-hydration model for the early-age elastic properties of cement-based materials, Cement and Concrete Research 33 (2003) 1293–1309.
[3] K. Fuji, W. Kondo, Kinetics of the hydration of tricalcium silicate, Journal of the American Ceramic Society 57 (1974) 492–502.
[4] U. Schneider, H. Bruckner, M. Oswald, Wiener Baustofflehre Blätter, Bindemittel, 13th Edition, Institute for Building Construction and Technology, Vienna University of Technology, Vienna, Austria, 2004 in German.
[5] R. Berliner, M. Popovici, K. Herwig, M. Berliner, H. Jennings, J. Thomas, Quasielastic neutron scattering study of the effect of water-to-cement ratio on the hydration kinetics of tricalcium silicate, Cement and Concrete Research 28 (2) (1998) 231–243.
[6] K.v. Breugel, Simulation of hydration and formation of structure in hardening cement-based materials, Ph.D. thesis, Delft University of Technology, Delft, The Netherlands (1991).
[7] G. Bye, Portland Cement, 2nd Edition, Thomas Telford Publishing, London, 1999.
[8] S. Goto, H. Fujimori, A. Hidaka, K. Ioku, Effects of components on the rate of heat liberation of the hydration in the system of glass/gypsum/lime, Journal of European Ceramic Society 26 (2006) 771–776.
[9] S. Song, H.M. Jennings, Pore solution chemistry of alkali-activated ground granulated blast-furnace slag, Cement and Concrete Research 29 (1999) 159–170.
[10] VDZ, Tätigkeitsbericht 2003-2005, Tech. rep., Verein Deutscher Zementwerke e. V., Forschungsinstitut der Zementindustrie, Düsseldorf, Germany, in German (2005).
[11] H. Brouwers, W. Chen, Hydration models for alkali-activated slag, in: E.V. Malhotra (Ed.), Proceedings 8th CANMET/ACI International Conferene on Fly Ash, Silica Fume, Slag, and Natural Pozzolans, Las Vegas, American Concrete Institute, Michigan, USA, 2004, pp. 303–318.
[12] A. Schindler, K. Folliard, Heat of hydration models for cementitious materials, ACI Materials Journal 102 (1) (2005) 24–33.
[13] S. Song, D. Sohn, H.M. Jennings, T.O. Mason, Hydration of alkali-activated ground granulated blast furnace slag, Journal of Materials Science 35 (2000) 249–257.
[14] P.W. Atkins, Physical Chemistry, 5th Edition, Oxford University Press, Oxford, England, 1994.